An Eikonal Approach for the Initiation of Reentrant Cardiac Propagation in Reaction-Diffusion Models

Vincent Jacquemet*

Published in IEEE Trans. Biomed. Eng. (2010), vol. 57, no. 9, pp. 2090-2098

***Abstract*— Microscale electrical propagation in the heart can be modeled by a reaction-diffusion system describing cell and tissue electrophysiology. Macroscale features of wavefront propagation can be reproduced by an eikonal model, a reduced formulation involving only wavefront shape. In this paper, these two approaches are combined to incorporate global information about reentrant pathways into a reaction-diffusion model. The eikonal-diffusion formulation is generalized to handle reentrant activation patterns and wavefront collisions. Boundary conditions are used to specify pathways of reentry. Finite-element-based numerical methods are presented to solve this non-linear equation on a coarse triangular mesh. The macroscale eikonal model serves to construct an initial condition for the microscale reaction-diffusion model. Electrical propagation simulated from this initial condition is then compared to the isochrones predicted by the eikonal model. Results in 2D and thin 3D test-case geometries demonstrate the ability of this technique to initiate anatomical and functional reentries along prescribed pathways, thus facilitating the development of dedicated models aimed at better understanding clinical case reports.**

I. Introduction

Computer models of the heart have been developed to describe the propagation of electrical excitation waves in the heart muscle using nonlinear partial differential equations of the reaction-diffusion type [1]. The construction of these models is based on a bottom-up approach, integrating biological data from ion channels to heart anatomy. Most available patient data (ECG, electrograms, electroanatomical mapping), however, provide a global, macroscale information with limited spatial resolution. In order to advance toward patient-specific modeling and improve the clinical relevance of simulation results, a top-down, multi-resolution approach is needed to incorporate patient-specific global information about the geometry and the dynamics of the arrhythmia [2]. A bottom-up approach would be used to develop a baseline model from single cell and tissue measurements, histological data and medical imaging [3], [4], while a top-down approach would be applied to adjust the baseline model to a patient and define an initial condition (i.e. the initial state of the cardiac cells) from global information about the dynamics of reentries such as pathways or activation times, based for instance on intracardiac electrograms.

Previous simulation studies in atrial models used programmed stimulation protocols to initiate reentries [5]–[8]. Narrow vulnerability windows often made the initiation protocols time-consuming. Forcing the wave fronts to follow reentrant circuits reported in clinical case studies was intricate. Repeating the simulations in another geometry usually required restarting the protocols from scratch. To facilitate these procedures, we aim to develop a computational framework for automatically initiating episodes of arrhythmia corresponding to reentrant dynamics with controllable preferential pathways. An original two-level approach will be used. At the coarse-grained level, a macroscopic propagation model (based on the eikonal equation) extrapolates measured or synthetic data (e.g. macroreentrant pathways) to reconstruct the activation sequence using a priori knowledge. At the fine-grained level, the full reaction-diffusion system is simulated. The coarse-grained model serves to define the initial condition for the fine-grained model.

In this paper, the mathematical framework and the computational methods of this approach are presented, as well as a numerical validation for 2D and 3D-surface test-case geometries. The results demonstrate that the initial guess obtained from the eikonal equation is sufficiently accurate to provide a simple and efficient way to initiate a reentry following a prescribed pathway in the reaction-diffusion model.

II. Methods

A. Monodomain Model of Cardiac Propagation

The propagation of the cardiac impulse in the myocardium can be described by the evolution of the membrane potential field $V_m(\mathbf{x},t)$. According to the monodomain theory, this evolution is governed by a reaction-diffusion equation [1]:

$$C_m \frac{\partial V_m}{\partial t} = \beta^{-1} \nabla \cdot \boldsymbol{\sigma} \nabla V_m - I_{\text{ion}} + I_{\text{stim}} \qquad (1)$$

where C_m is the membrane capacitance per unit area of membrane, β is the area of membrane per unit volume, and $\boldsymbol{\sigma}$ is the (effective) conductivity tensor. An externally driven stimulation current $I_{\text{stim}}(t)$ may be introduced. The ionic current flowing through the membrane (by convention, outward-oriented if positive), I_{ion}, depends not only on the voltage V_m but also on internal variables $\mathbf{q}$ (such as intracellular ionic concentrations or channel gate states) that satisfy a system of ordinary differential equations $\mathrm{d}\mathbf{q}/\mathrm{d}t = F_{\mathbf{q}}(V_m, \mathbf{q})$. No-flux boundary condition is assumed, i.e. $\mathbf{n} \cdot \boldsymbol{\sigma} \nabla V_m = 0$ where $\mathbf{n}$

This research is supported by the Natural Sciences and Engineering Research Council of Canada (NSERC).

V. Jacquemet is with Institut de Génie Biomédical & Département de Physiologie, Université de Montréal, and Hôpital du Sacré-Coeur de Montréal, Montréal, Canada.

The author thanks Alain Vinet (Université de Montréal) for helpful discussions and comments, the Lausanne Heart Group (Ecole Polytechnique Fédérale de Lausanne) for sharing simulation tools and the atrial geometry, and Craig S. Henriquez (Duke University) for making the CardioWave software package available.

is the unit vector normal to the boundary. An initial condition $V_m(\mathbf{x},0) = V_0(\mathbf{x})$ and $\mathbf{q}(\mathbf{x},0) = \mathbf{q}_0(\mathbf{x})$ is also needed.

In the next subsections, a method will be presented to design an initial condition leading to reentrant propagation along a predefined pathway. This initial condition will be constructed based on an approximation of cardiac activation provided by the eikonal-diffusion approach.

B. Eikonal-Diffusion Equation for Reentrant Activation

The eikonal-diffusion equation is an approximation of the monodomain propagation equation derived using singular perturbation techniques [9]–[11]. In this formulation, the activation map $\tau(\mathbf{x})$, i.e. the time τ at which the wave front passes through the point $\mathbf{x}$, is governed by an elliptic equation in the domain Ω where propagation occurs [10]:

$$c_0\sqrt{\nabla\tau\cdot\boldsymbol{\sigma}r_m\nabla\tau} - \nabla\cdot\boldsymbol{\sigma}r_m\nabla\tau = \tau_m \tag{2}$$

The parameters r_m and τ_m come from the linearization of the propagation equation around the resting potential: $r_m^{-1} = \beta\,\mathrm{d}I_{\mathrm{ion}}/\mathrm{d}V_m$ is the membrane conductance per unit volume at rest and $\tau_m = r_m\beta C_m$ is the membrane time constant. The dimensionless propagation speed c_0 is such that the conduction velocity of a planar wavefront is $c_0\sqrt{\sigma r_m}/\tau_m$ [10]. No-flux boundary conditions will be used (wave fronts propagate along the walls as a consequence of the boundary condition on V_m):

$$\mathbf{n}\cdot\boldsymbol{\sigma}\nabla\tau(\mathbf{x}) = 0\ , \quad \mathbf{x}\in\partial\Omega, \tag{3}$$

where $\partial\Omega$ is the domain boundary and $\mathbf{n}$ the unit vector normal to the boundary.

Equation (2) is still valid for a reentrant activation. In this case, τ will be normalized by the cycle length T (period) so that the scaled activation time $\hat\tau = 2\pi\tau/T$ ranges from 0 to 2π. To solve the phase unwrapping problem, the transform $\phi = \exp(i\hat\tau)$ is applied, leading to the equation:

$$\|\mathbf{c}\nabla\phi\| = 1 + \mathrm{Im}\,\nabla\cdot(\phi^*\mathbf{D}\nabla\phi)\ , \tag{4}$$

where the symmetric positive definite tensors $\mathbf{c}$ and $\mathbf{D}$ are defined by the relations:

$$\mathbf{c}^*\mathbf{c} = \frac{T^2}{4\pi^2}\,\frac{r_m c_0^2}{\tau_m^2}\,\boldsymbol{\sigma} \qquad \text{and} \qquad \mathbf{D} = \frac{T}{2\pi\beta C_m}\,\boldsymbol{\sigma}\ . \tag{5}$$

The symbol 'Im' denotes the imaginary part, $\|\cdot\|$ is the euclidean norm and the star $(*)$ means the conjugate (when applicable) transposed tensor. The boundary condition becomes $\mathbf{n}\cdot\mathbf{D}\nabla\phi(\mathbf{x}) = 0$ for $\mathbf{x}\in\partial\Omega$. In addition, the constraint $|\phi(\mathbf{x})| = 1$ must hold for $\mathbf{x}\in\Omega$.

The tensor $\mathbf{c}$ represents the normalized, possibly anisotropic, baseline propagation velocity (in cm/rad) and $\mathbf{D}$ (in cm^2) describes the diffusion process that creates curvature-dependent propagation velocity. The diffusion term also improves numerical stability and avoids non-uniqueness of the solution [10]. Despite the relation $\mathbf{c}^*\mathbf{c} = (c_0^2T/2\pi\tau_m)\,\mathbf{D}$, the parameters $\mathbf{c}$ and $\mathbf{D}$ will be kept formally independent in the next subsection to facilitate generalizations involving the limits $D\to 0$ (Subsect. III-A) and $D\to\infty$ (Subsect. III-C) with $\mathbf{c}$ fixed.

To simulate a reentry along a pathway of length L with a cardiac cell model with an effective refractory period ERP, a target cycle length $T > ERP$ is selected and the target conduction velocity CV is computed as $CV = L/T$. The period T should be adjusted (based on previous knowledge about the cell model) to result in a realistic excitable gap ($T - ERP$) and avoid unstable behavior. Equivalently, CV could be chosen within physiological range and T computed as L/CV provided that $T > ERP$. Then, the value of σ is adjusted to reproduce the target CV in the monodomain model. The scaled conduction velocity c is set to $L/2\pi$ and the diffusion coefficient to $D = T\sigma/2\pi\beta C_m$. Further adjustments of D may be needed to correct inaccuracies in the estimation of T and to account for discretization errors in the monodomain model leading to a nonlinear relationship between CV and $\sqrt{\sigma}$.

C. Discretized Linearized Eikonal-Diffusion Equation

The periodic nature of the solution prevents the use of fast-marching method [11]–[13] to numerically solve Eq. (4). Newton's root finding method (a natural extension of the linearized eikonal method [14]) will be applied at the PDE level [15, chap. 4] to the nonlinear functional equation

$$\mathcal{F}[\phi(\mathbf{x})] = \|\mathbf{c}\nabla\phi\| - \mathrm{Im}\,\nabla\cdot(\phi^*\mathbf{D}\nabla\phi) - 1 = 0\ . \tag{6}$$

Assuming that $\phi^0 = \exp(i\hat\tau^0)$ is an initial estimate of the solution (respecting the boundary condition), the estimate $\phi^{s+1} = \exp(i\hat\tau^{s+1})$ at step $s+1$ is obtained by computing a correction $\theta^s = \hat\tau^{s+1} - \hat\tau^s$ that satisfies the equation

$$\mathcal{F}\left[\exp(i\hat\tau^s)\right] + \frac{\mathrm{d}}{\mathrm{d}\epsilon}\mathcal{F}\left[\exp(i\hat\tau^s + i\epsilon\theta^s)\right]\Big|_{\epsilon=0} = 0\ . \tag{7}$$

The second term is the first variation of $\mathcal{F}$ [16], generalizing the usual Newton update formula. Analytical calculations lead to the following linear equation for θ:

$$\begin{aligned}\|\mathbf{c}\nabla\phi\| - \mathrm{Im}\,\nabla\cdot(\phi^*\mathbf{D}\nabla\phi) - 1 = \\ \|\mathbf{c}\nabla\phi\|^{-1}\ \mathrm{Im}\ (\phi\nabla\phi^*\mathbf{c}^*\mathbf{c}\nabla\theta) + \nabla\cdot(\mathbf{D}\nabla\theta)\end{aligned} \tag{8}$$

where the indices s were dropped for the sake of simplicity. The boundary condition remains $\mathbf{n}\cdot\mathbf{D}\nabla\theta = 0$.

Equation (8) is a steady-state convection-diffusion equation of the form:

$$\nabla\cdot(\mathbf{D}\nabla\theta) + \mathbf{b}\cdot\nabla\theta = f + \nabla\cdot\mathbf{F} \tag{9}$$

where the fields $\mathbf{b}$, $\mathbf{F}$ and f are known:

$$\begin{aligned}&\mathbf{b} = \|\mathbf{c}\nabla\phi\|^{-1}\ \mathrm{Im}\ (\phi\nabla\phi^*\mathbf{c}^*\mathbf{c})\ ,\\ &\mathbf{F} = -\mathrm{Im}\,(\phi^*\mathbf{D}\nabla\phi) \quad \text{and} \quad f = \|\mathbf{c}\nabla\phi\| - 1\ .\end{aligned} \tag{10}$$

The two-dimensional domain Ω is discretized using a triangular mesh composed of n_t triangles and n_v vertices. The set of triangles is denoted by $\mathcal{T}$ and the set of vertices by $\mathcal{V}$. Vertex $i\in\mathcal{V}$ is located at position $\mathbf{x}_i$. The triangle $(ijk)\in\mathcal{T}$ is denoted by T_{ijk} and its area by Ω_{ijk}. Linear shape functions N_i are used to reconstruct the fields ϕ and θ by interpolation ($N_i(\mathbf{x}_j) = \delta_{ij}$, the Kronecker symbol):

$$\phi = \sum_{i\in\mathcal{V}}\phi_i N_i \qquad \text{and} \qquad \theta = \sum_{i\in\mathcal{V}}\theta_i N_i \tag{11}$$

Following a Galerkin finite element approach, Eq. (9) is multiplied by each of the shape function N_m, integrated over

the domain Ω and the divergence theorem is applied. For each $m \in V$, we have:

$$\sum_{n\in\mathcal{V}} \int_\Omega \mathrm{d}\Omega \Big(-\nabla N_m \cdot (\mathbf{D}\nabla N_n) + \mathbf{b} N_m \cdot \nabla N_n \Big) \theta_n = \int_\Omega (f N_m - \mathbf{F}\cdot\nabla N_m)\mathrm{d}\Omega \quad (12)$$

This set of equations forms a linear system $\mathbf{A}\boldsymbol{\theta} = \mathbf{f}$ whose components are assembled element-wise. In the triangle T_{ijk}, the tensors $\mathbf{c}$ and $\mathbf{D}$ are assumed to have a constant value $\mathbf{c}_{ijk}$ and $\mathbf{D}_{ijk}$. Because linear shape functions are used, gradients are constant in each triangle. The operator ∇_{ijk} will denote the gradient evaluated in T_{ijk} [17]. After the fields $\mathbf{b}$, $\mathbf{F}$ and f have been expressed in terms of the shape functions N_p, application of the formulas (valid when $m, p \in \{i, j, k\}$)

$$\int_{T_{ijk}} \mathrm{d}\Omega \; N_m = \frac{\Omega_{ijk}}{3} \qquad \text{and} \quad (13)$$

$$\int_{T_{ijk}} \mathrm{d}\Omega \; N_m N_p = \frac{\Omega_{ijk}}{12}(1+\delta_{mp}) \quad (14)$$

leads to explicit expressions for the matrix $\mathbf{A}$ and the right hand side $\mathbf{f}$:

$$A_{mn}(\phi) = -\sum_{(ijk)\in\mathcal{T}} \Omega_{ijk} \nabla_{ijk} N_m \cdot \mathbf{D}_{ijk} \nabla_{ijk} N_n + \sum_{(ijk)\in\mathcal{T}} \frac{\Omega_{ijk}}{3} \|\mathbf{c}_{ijk}\nabla_{ijk}\phi\|^{-1} \; \mathrm{Im}\; \frac{\phi_i+\phi_j+\phi_k+\phi_m}{4} \times (\mathbf{c}_{ijk}\nabla_{ijk}\phi)^* \cdot (\mathbf{c}_{ijk}\nabla_{ijk} N_n) \quad (15)$$

$$f_m(\phi) = \sum_{\substack{(ijk)\in\mathcal{T} \\ m\in\{ijk\}}} \frac{\Omega_{ijk}}{3} \left(\|\mathbf{c}_{ijk}\nabla_{ijk}\phi\| - 1 + 3\, \nabla_{ijk} N_m \cdot \mathrm{Im} \frac{\phi_i^* + \phi_j^* + \phi_k^*}{3} \mathbf{D}_{ijk} \nabla_{ijk}\phi \right). \quad (16)$$

This matrix and this vector have to be reevaluated at each iteration.

D. Initial Estimate of the Activation Map

The solution to the eikonal-diffusion equation (4) with no-flux boundary condition is not necessarily unique. Many reentrant patterns may be possible in a given substrate, for instance clockwise or counterclockwise rotation. On the other hand, if the propagation velocity c has a value incompatible with pathway length, periodic reentrant activity may not be possible. Our proposed approach to address this issue consists in constructing by interpolation an initial estimate of the activation map that is compatible with the constraints and follows the desired pathways (denoted by Γ). Isochrone shape will be progressively corrected by successive iterations. Topological features (phase singularities or winding numbers) will be preserved throughout these iterations as long as the correction $\theta(\mathbf{x})$ does not include any phase singularity or non-zero winding number. A sufficient condition is that $\theta(\mathbf{x})$ is a smooth function with $|\theta| < \pi$.

The initial estimate ϕ^0 used to start Newton iterations will be constructed by solving the diffusion equation

$$\nabla \cdot \mathbf{D}\nabla\phi^0 = 0 \quad (17)$$

with boundary condition $\phi^0 = \phi_0$ on Γ and $\mathbf{n}\cdot\mathbf{D}\nabla\phi^0 = 0$ on the remaining part of the boundary $\partial\Omega \setminus \Gamma$. Typically, Γ will be a closed curve (a boundary or an obstacle) and $\phi_0 = \exp(2\pi i \ell / L)$ where ℓ is the curvilinear coordinate along Γ and L is the length of Γ. This specification will determine the choice for (normalized) propagation velocity $c = L/2\pi$. The initial estimate is a Laplacian interpolation [18] based on geometrical data (and possibly fiber orientation). Subsequent corrections (Newton iterations) will use a priori information about wavefront propagation.

Equation (17) is discretized using the first term in Eq. (15). To account for the Dirichlet boundary condition, the i-th row of the matrix equation is replaced for each $i \in \Gamma$ by the equation $\phi_i^0 = \phi_0(\mathbf{x}_i)$. The normalization constraint $|\phi^0| = 1$ is finally restored by dividing the solution ϕ^0 by its module.

E. Implementation of the Eikonal-Diffusion Solver

The eikonal-diffusion solver is described by the following algorithm:

1) Inputs: geometry (set of vertices $\mathcal{V}$ and triangles $\mathcal{T}$); conductive and diffusive properties ($\mathbf{c}$ and $\mathbf{D}$ defined on the set of triangles); specification of the initial estimate: Γ (subset of vertices) and the initial values ϕ_0 on Γ.
2) Initialization: compute and normalize ϕ^0 by solving Eq. (17)
3) Iterate for $s = 0, 1, 2, \ldots$ until $\|\theta\| < tol$
   a) Compute the matrix $\mathbf{A}(\phi^s)$ [Eq. (15)] and the vector $\mathbf{f}(\phi^s)$ [Eq. (16)]
   b) Solve the system $\left(\mathbf{A} - \frac{1}{n_v}\mathbf{e}\,\mathbf{e}^*\right)\boldsymbol{\theta} = \mathbf{f}$ using the biconjugate stabilized gradient method (BiCGstab) with incomplete LU preconditioner on $\mathbf{A}$; $\mathbf{e}$ is the n_v-by-1 vector containing 1 in each entry
   c) Underrelaxation: $\theta := \theta \cdot \min\left(1, \theta_{max}/\max(|\theta|)\right)$, where θ_{max} is a fixed parameter
   d) Set $\phi^{s+1} := \phi^s \exp(i\theta)$
4) Output: $\hat{\tau} := \arg \phi^{s+1}$

Note that the matrix $\mathbf{A}$ is singular since the sum of its columns is zero ($\mathbf{A}\mathbf{e} = \mathbf{0}$). As consequence, the reference of θ (location at which $\theta = 0$) has to be specified. A deflation method [19] was preferred (step 3b) in order to spread numerical error over the domain, notably in case of an inaccurate choice of propagation velocity parameter. Underrelaxation was necessary during the first iterations to prevent too large changes that would invalidate the assumption $\theta \ll 1$. The tolerance tol was set to 10^{-10} and the underrelaxation threshold θ_{max} to 0.1. Convergence was typically reached after 15 to 30 iterations. Implementation was performed in MATLAB using sparse matrix operations. At step 3b, although the matrix is fully populated, the linear solver only requires the ability to compute $\left(\mathbf{A} - n_v^{-1}\mathbf{e}\,\mathbf{e}^*\right)\boldsymbol{\theta}$ as a function of $\boldsymbol{\theta}$, which can be implemented as $\mathbf{A}\boldsymbol{\theta} - \mathrm{mean}(\theta)\cdot\mathbf{e}$.

F. Initial Condition for the Monodomain Model

Once the scaled activation pattern $\hat{\tau}(\mathbf{x})$ has been computed, an initial condition for the monodomain model can be constructed. The period T of the reentry is first estimated based on refractory period and wavelength considerations (Subsect. II-B). Cardiac propagation is then simulated in a one-dimensional cable (length: 1 cm; space step: 0.1 mm) with the same conduction (average longitudinal conductivity) and membrane properties as the complete monodomain model. A stimulus current is injected at an extremity of the cable to elicit a train of electrical waves at a basic cycle length of T. Once steady state is reached, the evolution of the state of the midpoint of the cable is recorded and is denoted by $V_{\mathrm{paced}}(t)$ and $\mathbf{q}_{\mathrm{paced}}(t)$. Baring alternans or dynamical instability, these functions are expected to be periodic of period T. The initial condition associated with an activation map $\hat{\tau}(\mathbf{x})$ is defined as $V_0(\mathbf{x}) = V_{\mathrm{paced}}(t(\mathbf{x}))$ and $\mathbf{q}_0(\mathbf{x}) = \mathbf{q}_{\mathrm{paced}}(t(\mathbf{x}))$, where $t(\mathbf{x}) = T\cdot(1-\hat{\tau}(\mathbf{x})/2\pi)$. Implementing this operation requires both space and time interpolation. Linear time interpolation and nearest-neighbor spatial interpolation were applied.

G. Test Cases

Three test-case geometries were used to validate the approach: an annulus, a schematic representation of a ventricular slice and a simplified surface model of the human atria. Two-dimensional triangular meshes were generated using TRIANGLE by J. R. Shewchuk [20] and surface meshes using VRMESH (VirtualGrid, Seattle City, WA). For the annulus (inner radius: 2 cm; outer radius: 5 cm), 6 triangular meshes were generated with a number of nodes ranging from 563 ($\Delta x = 4$ mm) to 10,451 ($\Delta x = 0.9$ mm). A coarse (5,050 nodes, $\Delta x = 0.82$ mm) and a fine mesh (32,820 nodes, $\Delta x = 0.32$ mm) of the ventricular slice were created. The atrial epicardium was represented by a triangular surface mesh (13,798 nodes, $\Delta x = 1.2$ mm). In order to run reaction–diffusion simulations in 3D, a cubic mesh (748,741 nodes, $\Delta x = 0.33$ mm, thickness ≈ 1.6 mm) was created to represent the atrial working myocardium. The coarse atrial surface model lied within the bulk of the 3D model to enable data extrapolation from 3D-surface to full 3D.

Monodomain simulations were run from initial conditions generated by the eikonal-diffusion approach. The tensors $\mathbf{c}$ and $\mathbf{D}$ used by the eikonal-diffusion solver were set to values corresponding to the tissue properties specified in the monodomain model [Eq. (5)]. The Luo–Rudy [21] (for the ventricular slice) and the Courtemanche *et al.* [22] membrane kinetics (for the atrial model) were used. Monodomain equations were solved using finite volume discretization and forward Euler numerical scheme implemented in the software package CARDIOWAVE [23] as well as in a custom software developed previously [7], [24]. Activation time was identified as the time at which V_m crosses the threshold -60 mV when the time derivative of V_m is positive. Activation maps after 4 to 6 periods (turns) of the reentry were compared to the activation maps predicted by the eikonal-diffusion solver.

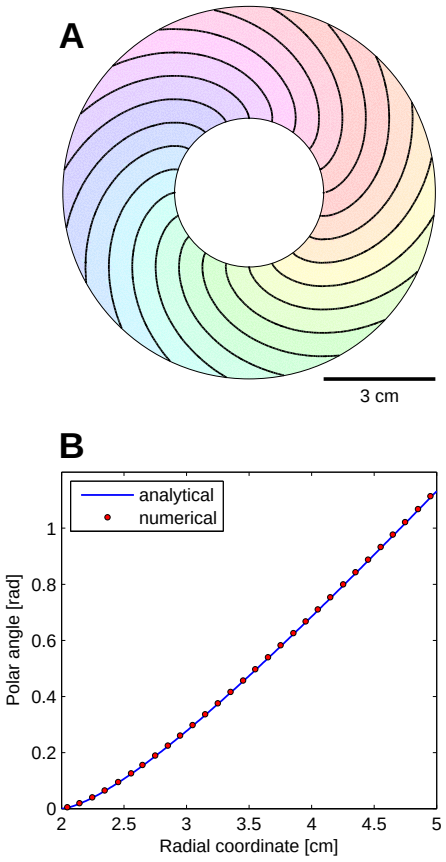

Fig. 1. Clockwise reentry in an annulus computed using the eikonal-diffusion approach. (A) Isochrones plotted every $1/20$ of cycle length. Activation time is color-coded. (B) Comparison of wavefront shape with an analytical formula (in polar coordinates).

III. RESULTS

A. Convergence of the Eikonal-Diffusion Solver

The convergence of the algorithm was verified in a geometry representing an annulus. In this case, the eikonal-diffusion equation can be solved analytically in the absence of diffusion ($D = 0$). The wavefront shape is an involute of a circle [25], described in polar coordinates (r, ϑ) by the equation (for clockwise rotation; parametrization from [26]):

$$\vartheta(r) = \tan(s) - s \quad \text{where} \quad s(r) = \arccos\frac{r_0}{r}\ . \qquad (18)$$

The parameter r_0 is the inner radius of the annulus.

To specify the initial estimate for the eikonal-diffusion problem, Γ was defined as the inner circle and $\phi_0(\vartheta) = \exp(-i\vartheta)$ on Γ in order to initiate a clockwise rotation (see Subsect. II-D). As a result, the initial estimate of ϕ was $\phi^0(r,\vartheta) = \exp(-i\vartheta)$ within the entire annulus. The propagation velocity was set to a uniform isotropic value $c = r_0$ and the diffusion constant was set to the smallest value $D = 0.0011$ cm^2 that still ensured numerical stability in the finest mesh (10,451 nodes). The resulting isochrones are plotted in Fig. 1A. In the eikonal-diffusion equation, diffusion of activation times operates at a space scale of $\sqrt{D}$. The boundary layer where the effect of boundary condition is prominent (isochrones

TABLE I

ROOT MEAN SQUARE ERROR IN WAVEFRONT SHAPE IN AN ANNULUS FOR DIFFERENT MESH RESOLUTIONS

#nodes	Δx	RMS error
563	4.0 mm	$1.6 \cdot 10^{-1}$ rad
901	3.1 mm	$4.0 \cdot 10^{-2}$ rad
1801	2.2 mm	$2.3 \cdot 10^{-2}$ rad
2664	1.8 mm	$1.1 \cdot 10^{-2}$ rad
5260	1.3 mm	$3.4 \cdot 10^{-3}$ rad
10451	0.9 mm	reference

orthogonal to the boundary) has a thickness of $\sqrt{D}$. Since here $\sqrt{D} = 0.37\,\Delta x$, this effect is not clearly visible on Fig. 1. Accuracy was assessed by computing the root mean square (RMS) error of the wavefront shape expressed in polar coordinates $\vartheta(r)$. Both curves (analytical and numerical) are shown in Fig. 1B. The RMS error was $4.1 \cdot 10^{-4}$ rad.

Mesh resolution was varied to estimate the spatial resolution required by the eikonal-diffusion solver. The diffusion coefficient was set to $D = 0.02$ cm^2 for all the meshes. Because this value of D was sufficient to create curvature-dependent propagation velocity, the results were compared to those of the finest mesh and not to the analytical formula (only valid for $D = 0$). The RMS errors are reported in Table I. Even for $\Delta x = 4$ mm, the solution is qualitatively correct. Most of the error is concentrated near the inner circle where wavefront curvature is maximal (where the radius of curvature becomes $< \Delta x$). A resolution of $\Delta x = 1$ to 2 mm gave sufficiently accurate results for most applications.

B. Comparison of Simulated Activation Maps

Activation maps were computed using both the eikonal-diffusion equation and the reaction-diffusion system in a geometry representing a ventricular slice with uniform conductive and diffusive properties to illustrate anatomical reentries and handling of wavefront collisions. The parameters of the monodomain equations were $C_m = 1$ μF/cm^2, $\beta = 2000$ cm^{-1}, $\sigma = 1.11$ mS/cm and $I_{\text{stim}} = 0$, and I_{ion} followed the formulation of the Luo–Rudy model.

The initial estimate for the eikonal-diffusion solver was computed using a Dirichlet boundary condition on the inner boundary (Γ) corresponding to the left ventricle: $\phi_0(\ell) = \exp(2\pi i \ell / L)$ where ℓ is the curvilinear coordinate along Γ in the clockwise direction and $L = 9.34$ cm is the length of Γ. To initiate a counterclockwise reentry, $\phi_0(\ell) = \exp(-2\pi i \ell / L)$ was used instead. The baseline conduction velocity in the monodomain model was $CV = 34.6$ cm/s for $\sigma = 1.11$ mS/cm. The estimated period was therefore $T = L/CV = 274$ ms, which is sufficiently long to ensure the stability of the reentry. The normalized propagation velocity was set to $c = L/2\pi$ and the diffusion coefficient to $D = T\sigma/2\pi\beta C_m = 0.024$ cm^2. The coarse mesh (5,050 nodes) was used. The resulting isochrones are shown as thick dashed lines in Fig. 2A (clockwise rotation) and Fig. 2B (counterclockwise rotation).

The activation map obtained through the eikonal-diffusion approach was used to create an initial condition for the reaction-diffusion model (Subsect. II-F). The fine mesh (32,820 nodes) was used in these monodomain simulations. Observed cycle lengths for the first 4 rotations was 270 ms, 269 ms, 268 ms and 268 ms for clockwise rotations and 272 ms, 270 ms, 269 ms and 269 ms for counterclockwise rotations. In successive rotations, activation patterns were almost identical, demonstrating that the initial condition was close to steady state. The resulting isochrones are shown as solid lines in Fig. 2. These isochrones coincide with those computed using the eikonal-diffusion equation on a coarse mesh, suggesting that this simplified approach reproduces realistic reentrant activations in the case of low curvature wavefronts in a uniform medium.

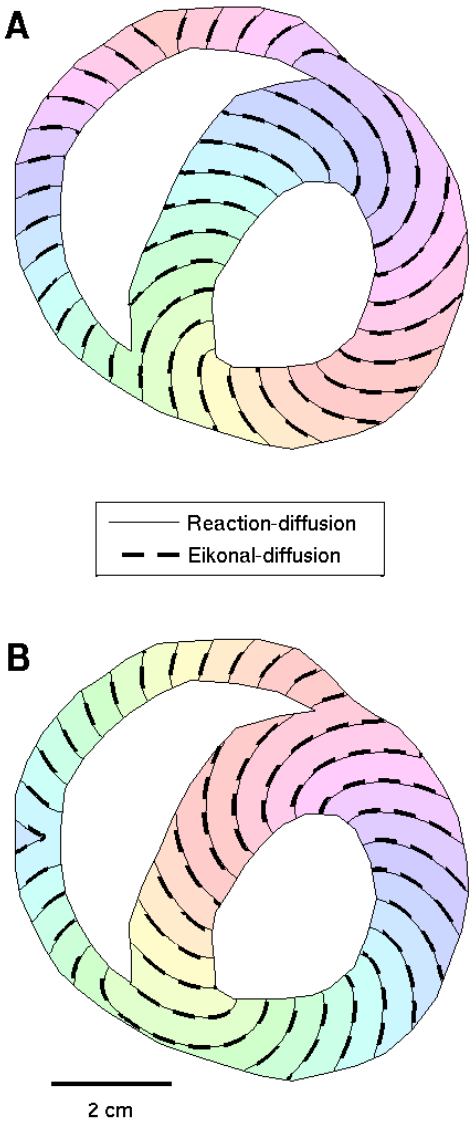

Fig. 2. Activation maps computed using the eikonal-diffusion approach (thick dashed lines) and the full reaction-diffusion system after four periods (solid lines). Isochrones are plotted every $1/20$ of cycle length. Activation time is color-coded. (A) clockwise rotation; (B) counterclockwise rotation.

C. Interpolation of Angle Fields

Fiber orientation will be introduced in the ventricular slice model to test the ability of the eikonal-diffusion method to account for anisotropic conduction (Subsect. III-D). Instead of integrating experimental fiber orientation, we will demonstrate how the eikonal-diffusion solver can be adapted for the interpolation of angle-valued fields.

Fiber angle $\alpha(\mathbf{x})$ in two-dimensional domain is defined modulo π. At the boundaries, α will be assumed to be parallel to the wall. This defines a Dirichlet boundary condition. Interpolation within the domain can be performed by solving the Laplacian equation $\Delta\alpha = 0$. This equation is equivalent to the isotropic eikonal-diffusion equation (2) for $\hat{\tau} = 2\alpha$ and $D \to \infty$. Practically, D is set to 1, c is set to 0, only the first term is kept in $\mathbf{A}$ [Eq. (15)] and the first term in the definition of $\mathbf{f}$ [Eq. (16)] is dropped. In addition, in the algorithm (Subsect. II-E) at step 4b, the Dirichlet boundary condition is enforced by replacing the equation of each row corresponding to a boundary node i by $\theta_i = 0$ (θ is the correction term). Once the solution $\hat{\tau}$ is obtained, α is set to $\hat{\tau}/2$. The resulting fiber angle field, displayed in Fig. 3A, demonstrates the ability to handle the angle unwrapping problem.

D. Anisotropic Conduction

In the 2D anisotropic case, the tensor fields $\mathbf{c}$ and $\mathbf{D}$ can be defined (in the x-y coordinate system) as a function of the fiber angle α using the function

$$\mathbf{T}(\alpha,\kappa) = \begin{pmatrix} \cos^2\alpha + \kappa^{-1}\sin^2\alpha & (1-\kappa^{-1})\sin\alpha\cos\alpha \\ (1-\kappa^{-1})\sin\alpha\cos\alpha & \sin^2\alpha + \kappa^{-1}\cos^2\alpha \end{pmatrix}.$$

The parameter $\kappa \geq 1$ is the anisotropy ratio (ratio between the largest and the smallest eigenvalue). Note that $\mathbf{T}(\alpha,\kappa_1)\mathbf{T}(\alpha,\kappa_2) = \mathbf{T}(\alpha,\kappa_1\kappa_2)$. More specifically, we can write $\mathbf{D}(\mathbf{x}) = D_l\ \mathbf{T}(\alpha(\mathbf{x}),\kappa_D)$ and $\mathbf{c}(\mathbf{x}) = c_l\ \mathbf{T}(\alpha(\mathbf{x}),\kappa_c)$ where D_l and c_l are the longitudinal diffusion coefficient and propagation velocity. Similarly, the conductivity tensor for the monodomain equation is written as $\boldsymbol{\sigma}(\mathbf{x}) = \sigma_l\ \mathbf{T}(\alpha(\mathbf{x}),\kappa_\sigma)$.

Following the same approach and using the same parameters as in Subsect. III-B, a clockwise reentry was initiated around the right ventricle in both the eikonal-diffusion and the reaction-diffusion models. Conduction properties were anisotropic with $\sigma_l = 2.23$ mS/cm, $\kappa_\sigma = 4$ and the fiber orientation shown in Fig. 3A. Pathway length ($L = 14.6$ cm) and (longitudinal) conduction velocity were both roughly 50% larger than in Subsect. III-B, so the same estimate for the period $T = 274$ ms was used. The normalized longitudinal propagation velocity was set to $c_l = L/2\pi$ and its anisotropy ratio to $\kappa_c = \sqrt{\kappa_\sigma} = 2$. The longitudinal diffusion coefficient was set to $D_l = T\sigma_l/2\pi\beta C_m = 0.049$ cm^2 and its anisotropy ratio to $\kappa_D = \kappa_\sigma = 4$.

In the reaction-diffusion model, 6 rotations were simulated from the initial condition provided by the eikonal diffusion model. The resulting activation map is shown in Fig. 3B (solid lines). The cycle length of reentry was 267 ms at steady state and varied by less than 1 ms between the first to the sixth rotation. As commonly observed in monodomain simulations due to discretization errors, the propagation velocity was not exactly proportional to the square root or the conductivity. To account for this discrepancy, the activation map from the eikonal model was recomputed with the updated parameters $T = 267$ ms, $\kappa_c = 2.15$ and $\kappa_D = \kappa_c^2$, and displayed in Fig. 3B (thick dashed lines).

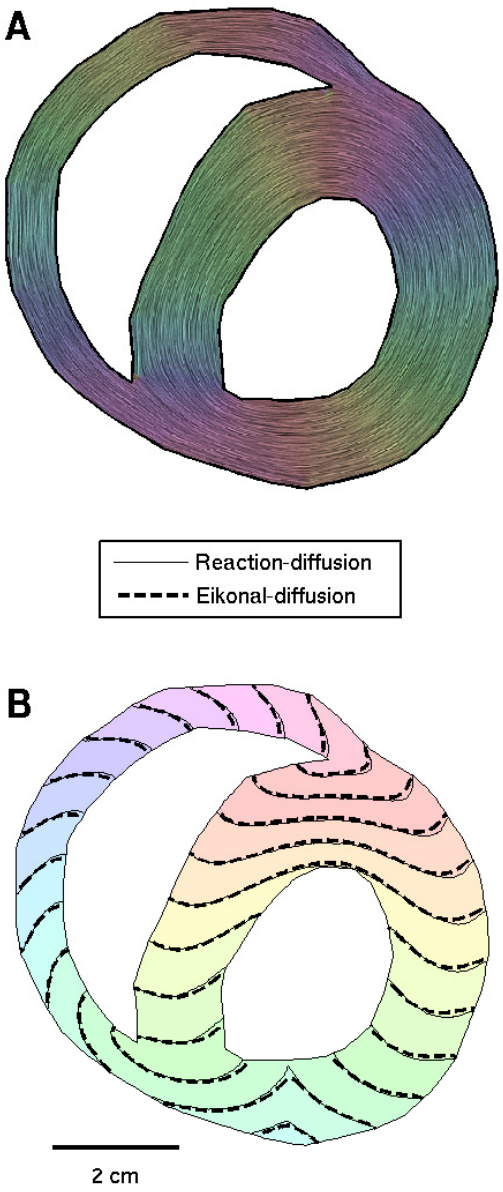

Fig. 3. (A) Example of fiber angle interpolation displayed as a texture generated by line integral convolution (using a custom code based on an implementation by W. Martin, Univ. of Utah). Fiber angle is color-coded in the range 0 to π. (B) Activation maps in an anisotropic medium computed using the eikonal-diffusion approach (thick dashed lines) and the full reaction-diffusion system after six periods (solid lines). Isochrones are plotted every $1/20$ of cycle length. Activation time is color-coded.

E. Anatomical and Functional Reentries

A simplified atrial geometry was used to investigate the initiation of reentries in a more complex topology. Activation maps were computed using both the eikonal-diffusion equation (3D-surface model) and the reaction-diffusion system (3D

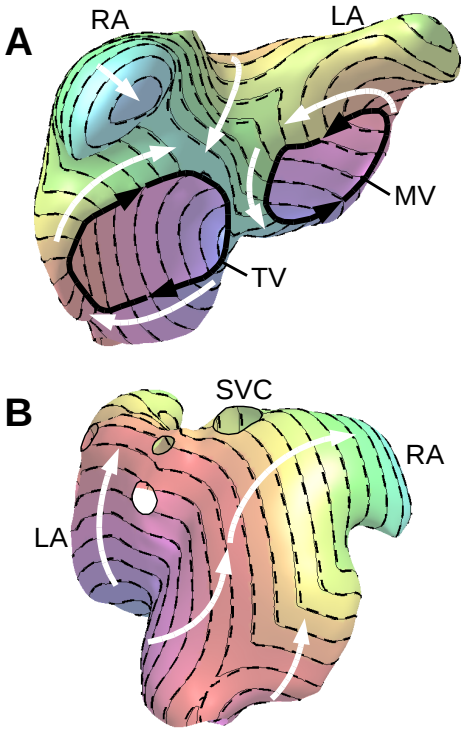

Fig. 4. Activation maps representing a figure-of-eight reentry in a simplified atrial model computed using the eikonal-diffusion approach in a surface mesh (thick dashed lines) and the full reaction-diffusion system in 3D after five periods (solid lines). Isochrones are plotted every $1/20$ of cycle length. Activation time is color-coded (and also displayed in the endocardium). White arrows illustrate wave front propagation and black arrows indicate the circuits that served as boundary condition Γ for the eikonal problem. (A) anterior view; (B) right-posterior view. RA: right atrium; LA: left atrium; TV: tricuspid valve; MV: mitral valve; SVC: superior vena cava.

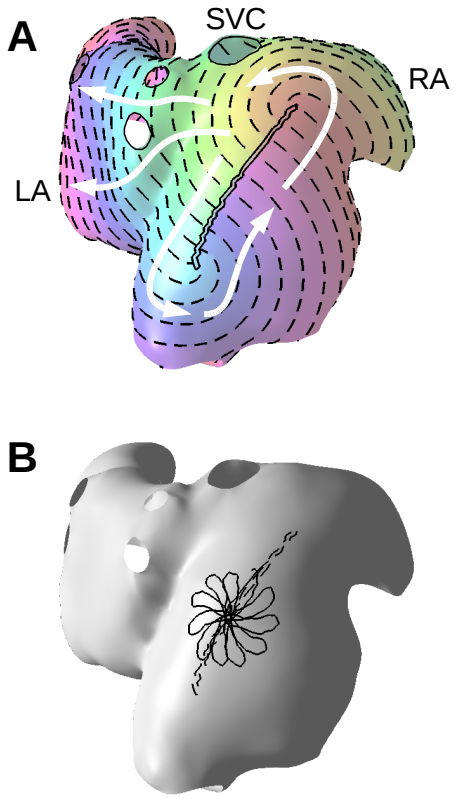

Fig. 5. (A) Reentry around an obstacle (solid line) computed using the eikonal-diffusion approach. Isochrones (dashed lines) are plotted every $1/20$ of cycle length. Activation time is color-coded. (B) Trajectory of the phase singularity of the reentry (solid line) simulated in the reaction-diffusion model when the obstacle (dashed line) is removed. RA: right atrium; LA: left atrium; SVC: superior vena cava.

model) with uniform conductive and diffusive properties.

1) Anatomical reentry: A figure-of-eight reentry was designed using the eikonal-diffusion approach: Γ was the boundary of the mitral valve (MV; length: L_{MV}) and the tricuspid valve (TV; length: L_{TV}), and ϕ_0 was set to $\exp(2\pi i\ell/L_{MV})$ and $\exp(-2\pi i\ell/L_{TV})$ respectively on the mitral and tricuspid boundary. The propagation velocity was set to $c = L_{MV}/2\pi$ and the diffusion coefficient to $D = 0.08$ cm^2 computed from the parameters $T = 240$ ms, $C_m = 1$ μF/cm^2, $\beta = 2000$ cm^{-1} and $\sigma = 4.2$ mS/cm. The resulting activation map, displayed as thick dashed lines in Fig. 4, served to define the initial condition for a simulation in a 3D reaction-diffusion system. The L-type calcium current in the Courtemanche model was inhibited by 75% to reduce action potential duration and rate adaptation and thus stabilize reentries [27]. The simulated reentrant patterns were stable from the first beats (with a period of 198 ms). Small differences in activation time (2–3 ms) between the eikonal-diffusion and reaction-diffusion results were observed, mostly at a collision site near the anatomical location of the septum (Fig. 4).

2) Functional reentry: In order to initiate a functional reentry at a predefined location, a line was drawn manually on the right atrium free wall using an interactive tool developed in MATLAB. Its length is aimed to be half of the wavelength. The triangles along the line were removed to create a new boundary Γ on which ϕ_0 was specified as previously. The activation map computed using the eikonal-diffusion equation is shown in Fig. 5A. The reentry simulated in the reaction-diffusion system evolving from this initial condition was not periodic but quasiperiodic. After a first cycle following the pattern predicted by the eikonal approach, the wave front meandered (the line introduced as obstacle was not present in the reaction-diffusion model). Wave front 3D propagation (scroll wave) can be described by a filament (tip of the spiral). Since the 3D model was thin, the filament was always short and was projected on the epicardium and called phase singularity. The trajectory of the phase singularity is represented in Fig. 5B. The phase singularity stayed in the vicinity of the desired location.

IV. Discussion

In previous works, eikonal equations have been successfully applied to predict paced or normal macroscopic propagation in the ventricles [9]–[11] and in the atria (in the form of the shortest path algorithm) [28]. The rationale of this simplified approach was the limited number of parameters involved and the very small computational requirements. Today's technol-

ogy enables the simulation of large-scale bidomain models at micro-resolution [3]. Despite these advances, reproducing in a cardiac propagation model an arrhythmia on the basis of the description of reentrant pathways from a clinical case report remains challenging. Chronic arrhythmias such as atrial fibrillation evolve over weeks or months and there is little hope to simulate all the process from the initial trigger to the chronic form of the arrhythmia. Instead our objective would be to capture the major features of wave front dynamics in a patient and integrate these data to create an initiation condition for the computer model.

This paper addresses this issue by extending the eikonal approach to reentrant activations and by creating a link between macroscopic propagation obtained on a coarse mesh and ionic model-based propagation in a detailed (possibly micro-scale) model. Lines et al. [2] proposed an alternative approach to synchronize a reentrant activity with experimental or synthetic signals recorded at sparse locations during flutter. Their reaction-diffusion model was run with an additional non-local forcing term resulting in the desired synchronization. In contrast, our method involves only activation times computed on a coarse mesh in the first step, and enables the initiation of quasiperiodic or unstable reentries (Fig. 5). When the cell model used features slow adaptation to sudden rhythm change (such as slow variations in ionic concentrations), another advantage is that the initial condition is already close to steady state. If a S_1–S_2 stimulation protocol was used instead, the premature stimulus might lead to a long transient period, possibly unstable (transient wave breaks).

Two different eikonal formulations have been derived in the literature: the eikonal-diffusion and the eikonal-curvature equations [9], [10], [29]. Their wavefront curvature-dependence of propagation velocity coincides up to first order in wavefront curvature [10]. At large wavefront curvature, only the eikonal-curvature equation correctly predicts propagation failure. On the other hand, only the eikonal-diffusion model accounts for boundary and collision effects on propagation. To avoid non-existence of the activation time in high-curvature regions and better handle boundary and collisions, the eikonal-diffusion formulation was selected. Figure 2 demonstrates that low-curvature wavefronts are almost identical in the eikonal-diffusion and in the reaction-diffusion systems. High wavefront curvature due to anisotropy and sharp angles in the boundary resulted in small inaccuracies in the isochrones (Fig. 3). Another source of error is the obvious inability to handle radius of curvature smaller than (coarse) mesh resolution. In its current implementation, the method is limited to 2D geometries or thin 3D models (like the atria). A 3D extension is however possible, as it was the case for paced propagation [10].

A method was presented to initiate a functional reentry at a prescribed location (Fig. 5). In this case, the assumption of a periodic reentrant activity is clearly wrong, but only serves to generate an appropriate initial condition. Indeed the eikonal model does not include any information about repolarization. Tissue parameters (conduction velocity, action potential duration, restitution) will determine the dynamical regime and the persistence or stability of the reentry [27]. Although spirals can also be initiated using cross-shock stimulation, our approach can be extended to multiple spirals (fibrillation) or to multiarm spiral [30], allow to easily control the location of the other extremity of the wavefront, and do not require simulating the first activation in the reaction-diffusion model (before the second stimulus is delivered).

The same methodology can be applied to Laplacian interpolation of angular data or any variable defined modulo some constant (Fig. 3A), with a scope that extends well beyond fiber orientation. Another application of the eikonal-diffusion approach is direct computation of ECG based on activation maps [31]. This would provide a near-real-time research and educational tool similar to ECGSIM [32], extended for flutter-like reentries.

V. Conclusion

Along with the development of detailed microstructure models of cardiac electrophysiology, multiscale approaches become increasingly valuable. This paper presents a reliable, multiscale, computationally efficient and reasonably accurate tool for facilitating the initiation of reentry in ionic-based propagation models. This tool would help in the creation of a library of different types of simulated arrhythmias.

References

[1] R. Plonsey and R. C. Barr, *Bioelectricity: A Quantitative Approach*. Kluwer Academic Plenum Publishers, 2000.

[2] G. T. Lines, M. C. MacLachlan, S. Linge, and A. Tveito, "Synchronizing computer simulations with measurement data for a case of atrial flutter," *Ann Biomed Eng*, vol. 37, no. 7, pp. 1287–93, 2009.

[3] G. Plank, R. A. B. Burton, P. Hales, M. Bishop, T. Mansoori, M. O. Bernabeu, A. Garny, A. J. Prassl, C. Bollensdorff, F. Mason, F. Mahmood, B. Rodriguez, V. Grau, J. E. Schneider, D. Gavaghan, and P. Kohl, "Generation of histo-anatomically representative models of the individual heart: tools and application," *Philos Transact A Math Phys Eng Sci*, vol. 367, no. 1896, pp. 2257–92, 2009.

[4] V. Jacquemet, L. Kappenberger, and C. S. Henriquez, "Modeling atrial arrhythmias: Impact on clinical diagnosis and therapies," *IEEE Rev Biomed Eng*, vol. 1, pp. 94–114, 2008.

[5] Y. Gong, F. Xie, K. M. Stein, A. Garfinkel, C. A. Culianu, B. B. Lerman, and D. J. Christini, "Mechanism underlying initiation of paroxysmal atrial flutter/atrial fibrillation by ectopic foci: a simulation study," *Circulation*, vol. 115, no. 16, pp. 2094–102, 2007.

[6] E. J. Vigmond, R. Ruckdeschel, and N. Trayanova, "Reentry in a morphologically realistic atrial model," *J Cardiovasc Electrophysiol*, vol. 12, no. 9, pp. 1046–54, 2001.

[7] N. Virag, V. Jacquemet, C. S. Henriquez, S. Zozor, O. Blanc, J. M. Vesin, E. Pruvot, and L. Kappenberger, "Study of atrial arrhythmias in a computer model based on magnetic resonance images of human atria," *Chaos*, vol. 12, no. 3, pp. 754–763, 2002.

[8] M. Reumann, J. Bohnert, G. Seemann, B. Osswald, and O. Dossel, "Preventive ablation strategies in a biophysical model of atrial fibrillation based on realistic anatomical data," *IEEE Trans Biomed Eng*, vol. 55, no. 2 Pt 1, pp. 399–406, 2008.

[9] P. C. Franzone, L. Guerri, and S. Rovida, "Wave-front propagation in an activation model of the anisotropic cardiac tissue - asymptotic analysis and numerical simulations," *J Math Biol*, vol. 28, no. 2, pp. 121–176, 1990.

[10] K. A. Tomlinson, P. J. Hunter, and A. J. Pullan, "A finite element method for an eikonal equation model of myocardial excitation wavefront propagation," *SIAM J Appl Math*, vol. 63, no. 1, pp. 324–350, 2002.

[11] M. Sermesant, Y. Coudiere, V. Moreau-Villeger, K. S. Rhode, D. L. G. Hill, and R. S. Razavi, "A fast-marching approach to cardiac electrophysiology simulation for XMR interventional imaging," *Proc. MICCAI*, vol. 3750, pp. 607–615, 2005.

[12] T. J. Barth and J. A. Sethian, "Numerical schemes for the Hamilton-Jacobi and level set equations on triangulated domains," *J Comput Phys*, vol. 145, no. 1, pp. 1–40, 1998.

[13] J. Qian, Y.-T. Zhang, and H.-K. Zhao, "Fast sweeping methods for eikonal equations on triangular meshes," *SIAM J. Numer. Anal.*, vol. 45, no. 1, pp. 83–107, 2007.

[14] T. Alkhalifah, "Traveltime computation with the linearized eikonal equation for anisotropic media," *Geophys Prospect*, vol. 50, no. 4, pp. 373–382, 2002.

[15] H. P. Langtangen, *Computational Partial Differential Equations – Numerical Methods and Diffpack Programming*, ser. Texts in Computational Science and Engineering. Springer, 2003, vol. 1.

[16] H. Sagan, *Introduction to the calculus of variations*. New York: McGraw Hill, 1969.

[17] V. Jacquemet and C. S. Henriquez, "Finite volume stiffness matrix for solving anisotropic cardiac propagation in 2-D and 3-D unstructured meshes," *IEEE Trans Biomed Eng*, vol. 52, no. 8, pp. 1490–2, 2005.

[18] T. Oostendorp, A. van Oosterom, and G. Huiskamp, "Interpolation on a triangulated 3D surface," *J Comput Phys*, vol. 80, no. 2, pp. 331–343, 1989.

[19] M. S. Lynn and W. P. Timlake, "The use of multiple deflations in the numerical solution of singular systems of equations to potential theory," *SIAM. J. Numer. Anal.*, vol. 5, pp. 303–322, 1968.

[20] J. R. Shewchuk, "Triangle: Engineering a 2D quality mesh generator and Delaunay triangulator," in *Applied Computational Geometry: Towards Geometric Engineering*, ser. Lecture Notes in Computer Science, M. C. Lin and D. Manocha, Eds. Springer-Verlag, May 1996, vol. 1148, pp. 203–222, from the First ACM Workshop on Applied Computational Geometry.

[21] C.-H. Luo and Y. Rudy, "A model of the ventricular cardiac action potential," *Circ. Res.*, vol. 68, no. 6, pp. 1501–1526, June 1991.

[22] M. Courtemanche, R. J. Ramirez, and S. Nattel, "Ionic mechanisms underlying human atrial action potential properties: insights from a mathematical model," *Am J Physiol*, vol. 275, no. 1 Pt 2, pp. H301–21, 1998.

[23] J. B. Pormann, "A modular simulation system for the bidomain equations," Ph.D. dissertation, Duke University, Durham, NC, 1999.

[24] V. Jacquemet, A. van Oosterom, J. M. Vesin, and L. Kappenberger, "Analysis of electrocardiograms during atrial fibrillation. a biophysical model approach," *IEEE Eng Med Biol Mag*, vol. 25, no. 6, pp. 79–88, 2006.

[25] J. P. Keener and J. Sneyd, *Mathematical Physiology*, 2nd ed., ser. Interdisciplinary applied mathematics ; v. 8. New York: Springer, 2001.

[26] H. Josephs and R. L. Huston, *Dynamics of mechanical systems*. Boca Raton, FL: CRC Press, 2002.

[27] F. Xie, Z. Qu, A. Garfinkel, and J. N. Weiss, "Electrical refractory period restitution and spiral wave reentry in simulated cardiac tissue," *Am J Physiol Heart Circ Physiol*, vol. 283, no. 1, pp. H448–60, 2002.

[28] P. M. van Dam and A. van Oosterom, "Atrial excitation assuming uniform propagation," *J Cardiovasc Electrophysiol*, vol. 14, no. 10 Suppl, pp. S166–71, 2003.

[29] J. P. Keener, "An eikonal-curvature equation for action potential propagation in myocardium," *J Math Biol*, vol. 29, no. 7, pp. 629–51, 1991.

[30] N. Bursac, F. Aguel, and L. Tung, "Multiarm spirals in a two-dimensional cardiac substrate," *Proc Natl Acad Sci U S A*, vol. 101, no. 43, pp. 15 530–4, 2004.

[31] A. van Oosterom and V. Jacquemet, "Genesis of the P wave: atrial signals as generated by the equivalent double layer source model," *Europace*, vol. 7 Suppl 2, pp. 21–9, 2005.

[32] A. van Oosterom and T. F. Oostendorp, "ECGSIM: an interactive tool for studying the genesis of QRST waveforms," *Heart*, vol. 90, no. 2, pp. 165–8, 2004.

Vincent Jacquemet received the M.S. degree in physics in 2000 from the Swiss Federal Institute of Technology, Lausanne (EPFL), Switzerland, and the Ph.D. degree in biomedical engineering in 2004 from the Signal Processing Institute of EPFL. The topic of his thesis was the development of biophysical models of atrial fibrillation. Then he worked as a postdoc researcher in the Lausanne Heart Group at EPFL. Between 2007 and 2009, he was with the Department of Biomedical Engineering at Duke University with a "fellowship for advanced researcher" awarded by the Swiss National Science Foundation. Since 2009, he is researcher at Université de Montréal and Hôpital du Sacré-Coeur de Montréal. His research interests include complex dynamical systems, biophysical modeling, numerical simulation and signal processing.